https://doi.org/10.5194/egusphere-2022-1006
Preprint. Discussion started: 30 September 2022


# Peatlands and their carbon dynamics in northern high latitudes from 1990 to 2300: A process-based biogeochemistry model analysis

Bailu Zhao[1], Qianlai Zhuang[1, 2]
[1] Department of Earth, Atmospheric, and Planetary Sciences, Purdue University, West Lafayette, IN 47907, USA
[2] Department of Agronomy, Purdue University, West Lafayette, IN 47907, USA

*Correspondence to*: Qianlai Zhuang (qzhuang@purdue.edu)

**Abstract.** Northern peatlands are a large C sink during the Holocene, but whether they will keep being a C sink under future climate change is uncertain. This study simulates the responses of northern peatlands to future climate until 2300 with a Peatland version Terrestrial Ecosystem Model (PTEM). The simulations are driven with two sets of CMIP5 climate data (IPSL-CM5A-LR and bcc-csm1-1) under three warming scenarios (RCP2.6, 4.5 and 8.5). Peatlands expansion, shrink, accumulation and decomposition are modeled. In the 21st century, northern peatlands are projected to be a C source of 1.2-13.3 Pg C under all climate scenarios except for RCP 2.6 of bcc-csm1-1 (a sink of 0.8 Pg C). During 2100-2300, northern peatlands under all scenarios are a C source under IPSL-CM5A-LR scenarios, being larger sources than bcc-csm1-1 scenarios (5.9-118.3 vs. 0.7-87.6 Pg C). The peatland being C sources are due to: 1) water table depth (WTD) becomes deeper and permafrost thaw increases decomposition rate; 2) net primary production (NPP) does not increase much as climate warms because peat drying suppresses net N mineralization and 3) as WTD deepens, peatlands switches from moss-herbaceous dominated to moss-woody dominated, while woody plants require more N for productivity. Under IPSL-CM5A-LR scenarios, northern peatlands remain as a C sink until pan-Arctic annual temperature reaches -2.6 - -2.89°C, while this threshold is -2.09 - -2.35°C under bcc-csm1-1 scenarios. This study predicts an earlier northern peatland sink to source shift than previous estimates in the literature and emphasizes the vulnerability of northern peatlands to climate change.

## 1 Introduction

Peatlands are an ecosystem type that characteristically has more than 30cm peat thickness comprised of more than 30% organic materials within the peat layer. The formation of this thick organic soil layer requires wet and low oxygen conditions that prevent dead plant litter from fully decomposed (Finlayson and Milton, 2018). Around 85% of global peatlands C storage is in northern high latitude regions (415±150 Pg C) (Nichols and Peteet, 2019; Turunen et al., 2002) where low temperature and relatively high precipitation create favorable conditions for peat accumulation (Xu et al., 2018; Hugelius et al., 2020).

Peatlands are vulnerable to disturbances induced by climate warming (Loisel et al., 2021), especially when the warming in the Arctic region is more severe than in other regions (Allen et al., 2018). First, warming influences northern terrestrial ecosystem vegetation productivity by increasing spring photosynthesis and prolongs growing season (Piao et al.,

https://doi.org/10.5194/egusphere-2022-1006
Preprint. Discussion started: 30 September 2022


2008; Helbig et al., 2017). Second, warming could induce drier Arctic conditions (Finger Higgens et al., 2019), and peatlands water table drawdown will result in net increase of greenhouse gas emissions (Huang et al., 2021). Third, decomposition rate increases under higher temperature and previous studies found positive linear correlations between warming and net C loss rate (Hanson et al., 2020). Fourth, permafrost thaw under warming conditions will expose previously-frozen C for decomposition (Gandois et al., 2019). To date, multiple studies have explored northern peatland responses to future climate changes (Loisel et al., 2021; Qiu et al., 2020; Chaudhary et al., 2020; Müller and Joos, 2021). However, the projection of northern peatland C sink capacity during the 21st century is highly diverse including sink-to-source switch (Chaudhary et al., 2017; Müller and Joos, 2021), higher sink capacity under mild climate changes (Qiu et al., 2020), and the reduced C sink capacity (Chaudhary et al., 2020).

Given the uncertainties of northern peatlands response to future climate changes, modeling peatland C dynamics considering peatland extent changes could improve the accuracy of future projection. In this study, a process-base model, the Peatland Terrestrial Ecosystem Model (PTEM 2.2), is used to address this issue. PTEM 2.0 has been modified in terms of plant functional type (PFT), peat accumulation and decomposition, fen-bog transition and soil thermal module to better represent peatland ecosystem processes (Zhao et al., 2022b). The revised PTEM 2.0 is able to capture peat core age-depth profile at site level (Zhao et al., 2022b) and has been further modified and applied to simulate Holocene (PTEM 2.1, 15ka BP - 1990) pan-Arctic peatland accumulation and expansion at 0.5° resolution (Zhao et al., 2022a). The estimated pan-Arctic peatland C stock is 396-421 Pg C and Holocene average C accumulation rate (CAR) is 22.9 g C·m-2 yr-1 (Zhao et al., 2022a). The values and spatial pattern of soil C stock are in a close agreement with Qiu et al. (2019), Hugelius et al. (2020), Spahni et al. (2013) and Hugelius et al. (2013), and the values and temporal pattern of CAR are consistent with Loisel et al. (2014), Chaudhary et al. (2020) and Nichols and Peteet (2019). In this study, the results of the Holocene simulation are used as the initial condition for the future simulation.

The methods used in Holocene simulation can not be applied directly to future simulation due to two issues. First, previous studies on future peatland C dynamics are mostly based on fixed peatland extent (Loisel et al., 2021; Qiu et al., 2020; Chaudhary et al., 2020; Müller and Joos, 2021). However, the future peatland extent is likely to vary under climate change. To address this issue, we enhance PTEM 2.2 to simulate wetland dynamic extent during 1990-2300 at sub-grid cell scales. Notably, although the spatially explicit peat expansion process was considered in the Holocene simulation, the sub-grid cell expansion trend was simply derived from the fitted curve of existing pan-Arctic peat basal dates (Zhao et al., 2022a). It is problematic to apply this fitted trend to future simulation since severe climate changes may interrupt the Holocene peat expansion pattern. Therefore, a different approach of estimating peatland extent needs to be developed for future simulation.

Second, in PTEM 2.2, peatland water table depth (WTD) and nutrient availability is influenced by run-on. Previous PTEM 2.1 assumes run-on is a function of peat thickness and the theoretically maximum run-on when peat thickness is set to 0 cm. Under relatively stable climate conditions during the Holocene after peat initiation, the theoretically maximum run-on is assumed to be a constant (i.e., parameter) and thereby run-on solely depends on peat thickness (Zhao et al., 2022a).

However, when climate becomes wetter or drier in the future, the theoretically maximum run-on could vary significantly and the original PTEM 2.1 assumption becomes problematic. Therefore, it is necessary to revise the hydrology module of PTEM 2.2 such that run-on could respond to climate change.

To address these two issues, a TOPMODEL approach is used (Lu and Zhuang (2012). The TOPMODEL approach downscales coarse grid cell WTD into finer resolutions given the sub-grid-cell topographic wetness index (TWI) and decay parameter (*f*) (Beven and Kirkby, 1979). Previous studies have combined TEM, TOPMODEL and variable infiltration capacity (VIC) model to estimate Alaska Yukon river basin methane emissions using 1km resolution WTD interpolated from 30km resolution (e.g., Lu and Zhuang (2012)). By applying TOPMODEL, we are able to estimate the dynamics of a) sub-grid-cell WTD; b) the spatially explicit wetland fraction defined by annual WTD threshold (25cm, Fan et al. (2013)); c) sub grid-cell peat accumulation and decomposition given interpolated WTD; and d) the spatially explicit peatland fraction defined by peat thickness threshold (30cm, Finlayson and Milton (2018)). Furthermore, soil moisture can be estimated from WTD, with which we can estimate run-on from the difference between interpolated WTD and simulated WTD without run-on.

With peatland dynamics being simulated both horizontally (i.e., peatlands expansion and shrink) and vertically (i.e., peat accumulation and decomposition), this study aims to answer the following questions: a) how will the C sink of pan-Arctic peatlands change during 1990-2300? b) What are the major drivers for these changes? c) How does the pan-Arctic peatlands C sink respond to unit temperature and precipitation increase? and d) What is the threshold temperature and precipitation for pan-Arctic peatland C sink and source shift?

## 2 Methods

In this study, two CMIP5 climate model products (IPSL-CM5A-LR and bcc-csm1-1) are selected as climate inputs, with three warming scenarios considered (RCP 2.6, RCP 4.5 and RCP 8.5). The simulation is divided into two parts: 1) simulating grid cell average WTD with PTEM 2.2 and interpolating grid cell WTD into sub-grid cell scale with the TOPMODEL approach; and 2) simulating sub-grid cell scale peat accumulation and decomposition in current and potential peatland regions (Figure 1). Although this study aims at the peatland dynamics after 1990, the simulations start in 1940. The simulation during 1940-1990 works as spin up process and is also used for calibration against historical data.

### 2.1 Selection of climate input data

In the previous PTEM 2.0 site-level simulation, among many CMIP5 data products, IPSL-CM5A-LR product was selected as climate input because it provides long temporal coverage (1850-2300) for RCP 2.6, RCP 4.5 and RCP 8.5 scenarios (Zhao et al., 2022b). In addition, it shows a good agreement with CRU temperature in Eurasia and low biases in historical temperature and precipitation in North America (Miao et al., 2014; Sheffield et al., 2013). However, IPSL-CM5A-LR product also shows more extreme warming than the other CMIP5 products, especially under RCP 8.5 (Palmer et al., 2018). To address the uncertainty caused by climate inputs, another CMIP5 product, bcc-csm1-1, covering 1850-2300, three

https://doi.org/10.5194/egusphere-2022-1006
Preprint. Discussion started: 30 September 2022


RCP scenarios, projecting milder future climate warming, is selected. In order to run PTEM 2.2, temperature, precipitation, cloudiness and vapor pressure are required. Neither of IPSL-CM5A-LR and bcc-csm1-1 model provides vapor pressure data, which are thus calculated with temperature and relative humidity (Zhao et al., 2022b). Both climate products are bias-corrected to CRU data (v4.03, Harris et al. (2014)) during 1940-1990 as described in Zhao et al. (2022b). The bias correction makes sure that the difference in future simulations under two climate inputs are mostly introduced by the different level of post-1990 warming, rather than the difference in their historical records before 1990.

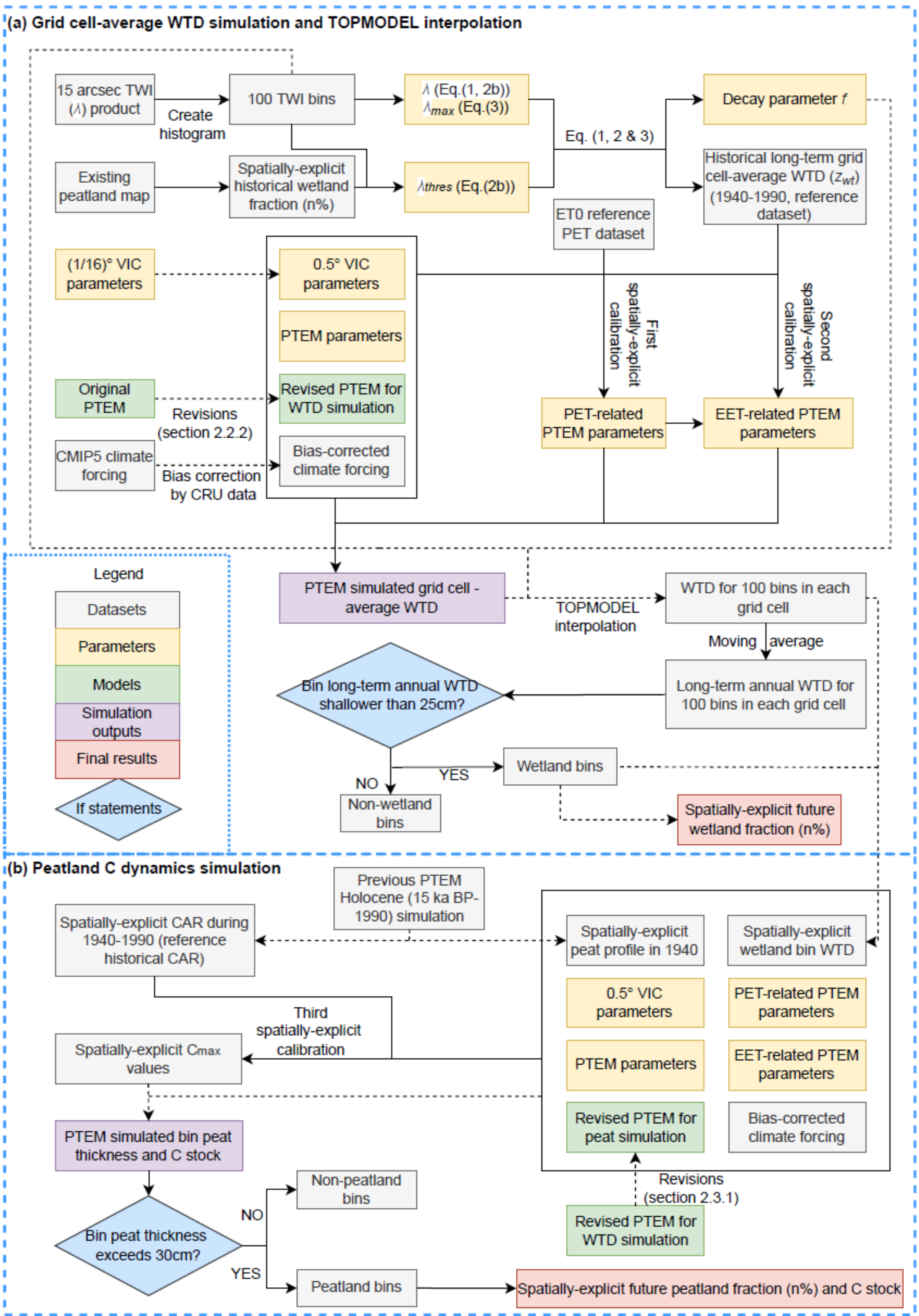


**Figure 1. Flow chart of Method Section 2.2 and 2.3.**

https://doi.org/10.5194/egusphere-2022-1006
Preprint. Discussion started: 30 September 2022


## 2.2 Future grid cell average WTD simulation

### 2.2.1 TOPMODEL parameter estimation

In this study, the peatland condition in 1940 derived from previous Holocene simulation is used as the initial condition for future peatland simulations (1940-2300) (Zhao et al., 2022a). In order to be consistent with the Holocene simulation, before running future WTD simulation, it is necessary to make sure that interpolating the PTEM-simulated recent WTD by TOPMODEL could derive the wetland extent as shown in the end of the Holocene simulation. In particular, 'recent' in this study refers to 1940-1990, and wetlands are defined as the region with long-term annual WTD shallower than 25cm (Fan et al., 2013). To satisfy this requirement, the TOPMODEL parameters need to be estimated before WTD simulation. TOPMODEL describes sub-grid cell WTD variation with topography. The topography effects on the local WTD are estimated with topographic wetness index (TWI) values, the larger TWI values indicate the shallower WTD and higher flooding probability (Stocker et al., 2014). In order to estimate sub-grid cell wetland and peatland conditions at 1% accuracy, each 0.5°×0.5° grid cell is divided into 100 bins by the TWI histogram (Figure 1 (a)). With global terrestrial TWI values available at 15 arcsec resolution (Marthews et al., 2015), each bin is composed of 36 TWI values where water bodies have null values. For bin *i* within a given grid cell:

$$z_{wti} = z_{wt} - \frac{1}{f} \times (k_i - \lambda) \quad (1)$$

Where $z_{wti}$ is the WTD of bin *i*, $k_i$ is the average TWI of bin *i*, λ is the grid cell average TWI, $z_{wt}$ is the grid cell average WTD and $f$ is the decay parameter. In Eq. (1), the parameters need to be estimated are $z_{wt}$ and $f$. In particular, the $z_{wt}$ here refers to the 50-year average WTD during 1940-1990. $z_{wt}$ and $f$ values are calculated as:

$$\begin{cases} f = 2.6 & (2a) \\ z_{wt-thres} = z_{wt} + \frac{1}{f}(\lambda_{thres} - \lambda) & (2b) \end{cases}$$

Where $f$ value is from Kleinen et al. (2020). $z_{wt-thres}$ is the threshold WTD of wetlands (i.e., -0.25m) and $\lambda_{thres}$ is the TWI value corresponding to $z_{wt-thres}$. For a given grid cell where wetland abundance is n% (n is an integer), $\lambda_{thres}$ is the TWI value of the n-th largest TWI values among 100 bins. The spatially explicit wetland fraction (n%) during 1940-1990 is consistent with the wetland fraction in 1990 in the Holocene simulation, which is the average value of three peatland maps covering the pan-Arctic region (Xu et al., 2018; Hugelius et al., 2020; Melton et al., 2022). The shallowest WTD in each grid cell is:

$$z_{wt-max} = z_{wt} + \frac{1}{f}(\lambda_{max} - \lambda) \quad (3)$$

Where $\lambda_{max}$ is the maximum TWI value in 100 bins. If $z_{wt-max}$ is greater than zero (i.e., above surface), $z_{wt-max}$ is assumed to be -0.01m, and $z_{wt}$ and $f$ values are calculated by Eq. (2b) and Eq. (3). Otherwise, $z_{wt}$ and $f$ values are calculated by Eq. (2a) and Eq. (2b).

### 2.2.2 PTEM revisions

The PTEM 2.1 used in pan-Arctic Holocene simulations is able to estimate the wetland WTD in a given grid cell, while not the grid-cell average WTD composed of both wetland and non-wetland land covers (Zhao et al., 2022a). In order to simulate the grid-cell average WTD, PTEM 2.1 is revised by applying some of the algorithms from VIC model. VIC model was developed by Liang et al. (1994) and has been updated to version 5 (VIC-5, Hamman et al. (2018)). Compared with the hydrology module of PTEM 2.1, VIC has the same soil vertical structure of three layers. The major hydrological processes including canopy interception of precipitation, infiltration, gravity-driven vertical flow, evapotranspiration, upper soil layer evaporation, effect of frozen-thaw on soil moisture are considered in both models (Liang et al., 1994; Zhuang et al., 2002). With similar structure, processes and variables, it is possible to apply some of VIC algorithms to PTEM 2.1. In particular, the algorithms of surface runoff, vertical flow from upper to lower layers, the computation of base flow and the estimation of WTD from given soil moisture are added to PTEM 2.1. The computation of surface runoff in VIC is based on the Xinanjiang model that assumes runoff is the amount of precipitation that falls on the saturated fraction of a grid cell (Zhao et al., 1980). The relationship between soil water storage and saturated fraction is given by:

$$i = i_m[1 - (1 - A)^{1/B}] \quad (4)$$

Where A is the fraction of the grid cell that the infiltration capacity (i.e., the possible maximum depth of water stored in soil column given area fraction) is less than $i$, $i_m$ is the maximum infiltration capacity within the given grid cell, and B is a shape parameter (Wood et al., 1992). The calculation of the uppermost layer runoff given precipitation and the initial soil moisture is well documented in Wood et al. (1992) (Eq. (1-3)) and Liang et al. (1994) (Eq. (13), Eq. (17-18)). In addition, gravity-driven water flow from upper to lower layers is given by Liang et al. (1994) (Eq. (18-20)) based on upper layer soil moisture, residual moisture content, pore size distribution index and the hydraulic conductivity estimated from Brooks (1965). Following VIC, PTEM 2.2 also assumes base flow only happens in the bottom soil layer. The computation of base flow in VIC is derived from the model in Franchini and Pacciani (1991) and the equations are listed in Liang et al. (1994) (Eq. (21)). Computing WTD given soil moisture was first used in VIC 4.1.2 (Bohn et al., 2013). Edited from VIC-5, the WTD-soil moisture relationship in PTEM 2.2 is given by:

$$W_{tot} = W_{avg} \times (SM_{max} - SM_{res}) + SM_{res} \quad (5)$$

Where $W_{tot}$ is the total soil moisture of three layers (mm), $W_{avg}$ is the average relative soil moisture, $SM_{max}$ is the maximum soil moisture (mm) and $SM_{res}$ is the residual soil moisture (mm). With $SM_{max}$ and $SM_{res}$ being spatially explicit parameters, $W_{avg}$ is:

$$W_{avg} = (D_{tot} - z_{wt} - \frac{b}{b-1} \times bubble \times (1 - \left(\frac{z_{wt}+bubble}{bubble}\right)^{\frac{b-1}{b}}))/D_{tot} \quad (6)$$

Where $D_{tot}$ is the total depth of soil layer (cm), $z_{wt}$ is given WTD (cm below surface), $bubble$ is the bubbling pressure (cm), $b$ is the parameter:

$$b = 0.5 \times (expt - 3) \quad (7)$$

Where $expt$ is the exponent parameter from Brooks-Corey relationship, and is always greater than 3 (Rawls et al., 1992). In PTEM 2.2, the spatially explicit relationship between WTD and total soil moisture is given by Eq. (5-7) at 5cm

WTD interval. During simulation, PTEM 2.2 calculates the total soil moisture and finds the corresponding WTD. In case of soil moisture does not correspond with any 5-cm interval WTD, PTEM 2.2 will find the closest upper and lower soil moisture values in the soil moisture-WTD profile and interpolate from the upper and lower WTD values.

In site-level and Holocene simulations, there are three PFTs in PTEM 2.0 and 2.1: moss, herbaceous plant and shrub (Zhao et al., 2022b). However, trees are also an important PFT in northern peatlands (Hanson et al., 2020). Therefore, in both grid-cell average WTD and sub-grid cell peatland simulations, it is necessary to include trees as a PFT. In particular, the vegetation C and N pool in PTEM 2.2 are now divided into four sub-pools: moss, herbaceous plant, shrub and tree. The dominance of these four PFTs are determined by WTD and their maximum possible productivity. The litter fall from four PFTs becomes the input of soil C and N, and the decomposition ability of litter is influenced by the fraction of litter origin from each PFT. The calculations of C and N cycles of trees are the same as the other three PFTs, although controlled by different PFT-specific parameters. The detailed description and equations are documented in Zhao et al. (2022b).

The calculation of evapotranspiration (EET) in PTEM 2.2 is derived from FAO algorithm for calculating crop EET (Allen et al., 1998):

$$EET = PET \times k_c \times foliage + E_{soil} \times (1 - foliage) \quad (8)$$

Where PET is the potential evapotranspiration given by Penman-Monteith model in PTEM 2.2, $k_c$ is a coefficient, $E_{soil}$ is the evaporation from bare land and $foliage$ is a PTEM 2.2 variable describing the relative abundance of leaf biomass (0-1). Although the FAO algorithm is widely applied in estimating crop EET, it is also proved applicable to shrubland, grassland and forest (Liu et al., 2017). In PTEM 2.2, $k_c$ is calculated as:

$$k_c = \sum_{i=1}^{3} k_{c-pft} \times w_{pft} \quad (9)$$

Where three vascular PFTs are considered influential to EET (i.e., herbaceous plant, shrub and tree), $k_{c-pft}$ is the spatially explicit coefficient for given PFT, and $w_{pft}$ is the weight of given PFT estimated from its dominance:

$$w_{pft} = \frac{VEGC_{pft}}{\sum_{i=1}^{3} VEGC_{pft}} \quad (10)$$

Where $VEGC_{pft}$ is the vegetation C of given PFT, and only three vascular PFTs are used for weight calculation. In WTD simulation, we assume no run-on from adjacent grid cells, thereby the grid cell water balance is:

$$\Delta SM = P - R_{off} - B - EET \quad (11)$$

Where $\Delta SM$ is the change of soil moisture, $P$ is precipitation, $R_{off}$ is surface run-off and $B$ is the bottom layer base flow.

### 2.2.3 Grid cell average WTD simulation and post-processing

Adding VIC algorithms to PTEM 2.2 requires VIC parameters at 0.5° resolution. These parameters include variable infiltration curve parameter (binfilt), maximum velocity of base flow (Dsmax), fraction of Dsmax where non-linear base flow begins (Ds), fraction of maximum soil moisture where non-linear base flow occurs (Ws), exponent used in base flow curve (c), expt in Eq. (7), saturated hydrologic conductivity (Ksat), depth of three soil layers (depth), bubbling pressure of soil layers (bubble), bulk density of soil layers (bulk_density) and soil particle density (soil_density). These parameter values are available globally at (1/16)° resolution (Schaperow and Li, 2021) and are aggregated into 0.5° resolution in this study. To run PTEM 2.2, in addition to the climate inputs, the historical (1940-1990) $CO_2$ concentration (ppm) is derived from TraCE 21ka dataset (He, 2011). The $CO_2$ concentration for three RCP scenarios (1991-2300) is provided by Meinshausen et al. (2011). Spatially explicit soil texture (Fao/Unesco, 1974) and elevation (Zhuang et al., 2002) were also required.

Before conducting WTD simulation, spatially explicit calibration for annual PET and $k_{c-pft}$ are conducted. Spatially explicit calibration for annual PET is conducted because the original PTEM 2.1 parameters estimate unreasonably large PET. Therefore, the global aridity index and potential evapo-transpiration (ET0) database v3 (Zomer and Trabucco, 2022) is selected as a reference. The dataset is selected because its annual PET is the long-term value of 1970-2000, which can be the approximate reference to the PET during 1940-1990 in this study. In addition, the reference dataset is also based on Penman-Monteith model but with more detailed estimation on the parameters than PTEM (Zomer and Trabucco, 2022). The 30 arcsec resolution reference PET is aggregated into 0.5° resolution for calibration. The spatially explicit Penman-Monteith parameters in PTEM 2.2 are calibrated with PEST (v17.2 for Linux). Since both reference dataset and PTEM 2.2 estimate PET with the same model, the calibration result is close to the reference for both IPSL-CM5A-LR and bcc-csm1-1 climate inputs (SI Figure 1).

After PET calibration, the spatially explicit calibration for $k_{c-pft}$ is conducted such that the 50-year WTD is consistent with the $z_{wt}$ calculated by Eq. (2-3). Same as PET calibration, spatially explicit $k_{c-pft}$ values are also calibrated by PEST (v17.2 for Linux). The wetland abundance in the end of the Holocene simulation (i.e., reference dataset) (Xu et al., 2018; Hugelius et al., 2020; Melton et al., 2022) and the wetland abundance interpolated by TOPMODEL from calibrated WTD (average of 1940-1990) is shown in SI Figure 2. Since each grid cell is divided into 100 bins by TWI values, the minimum wetland abundance is 1%. In this study, the grid cells with less than 1% wetland are not used for peat simulation. Leaving out the grid cells with less than 1% wetlands, the pan-Arctic wetlands area for the reference dataset is 2.93 $Mkm^2$, the calibrated wetlands area with IPSL-CM5A-LR forcing input is 2.81 million $km^2$, and with bcc-csm1-1 forcing input is 2.86 million $km^2$.

After calibration, the WTD simulation is conducted for 1940-2300 at 0.5° resolution (Figure 1 (a)). Notably, WTD simulation only aims at estimating grid cell average WTD and the peat accumulation and decomposition processes are not simulated. The grid cell average WTD during 1940-2300 is interpolated by TOPMODEL using the parameters calculated in Section 2.2.1. The changes of wetlands extent during 1990-2300 under IPSL-CM5A-LR and bcc-csm1-1 forcing inputs are presented in SI Figure 3 and 4.

## 2.3 Peatland simulation

### 2.3.1 PTEM revision

The TOPMODEL-interpolated bin WTD is used as an input in peatland simulation (Figure 1 (b)). In contrast to the WTD simulation where the grid cell run-on is assumed to be zero (Eq. (11)), the run-on in peatland simulation is calculated with a water balance equation:

$$\Delta SM = P + R_{on} - R_{off} - B - EET \tag{12}$$

Where $\Delta SM$ is the difference between soil moisture at two adjacent time steps (i.e., months), and the soil moisture in each month is estimated form the input WTD and the WTD-soil moisture relationship given by Eq. (5-7). The run-off ($R_{off}$), base flow ($B$) and evapotranspiration ($EET$) are calculated in the same way as in WTD simulation. In the Holocene simulation, soil pH value is calculated as a function of run-on which is solely controlled by peat thickness. In the revision, soil pH is calculated as:

$$pH = -log_{10}(n^{H^+}/SM) \tag{13}$$

Where $pH$ is the soil pH value, $n^{H^+}$ is the number of $H^+$ particles, and $SM$ is the soil moisture (mm). Notably, on unit area (i.e., $1m^2$), 1mm soil moisture is equal to 1L soil water. Therefore, $n^{H^+}/SM$ calculates the concentration of $H^+$ particles per liter. And the number of $H^+$ particles is calculated as:

$$\Delta H^+ = 10^{-pH_p} \times P + 10^{-pH_{ron}} \times R_{on} - 10^{-pH_w} \times EET - 10^{-pH_0} \times (R_{off} + B) \tag{14}$$

Where $pH_p$ is the pH value of precipitation (assumed 5.0), $pH_{ron}$ is the pH value of run-on water (assumed 7.0), $pH_w$ is the pH value of EET water (assumed 7.0), and $pH_0$ is the pH value of soil water at previous month. The spatially explicit initial pH values are from (Carter and Scholes, 2000).

In Holocene simulations, $CH_4$ production is simulated, but since oxidation process is not considered, $CH_4$ emission is not calculated. In this revision, $CH_4$ oxidation is enabled and thereby it is possible to estimate net $CH_4$ emission. The algorithms are documented in Zhuang et al. (2004).

**2.3.2 PTEM simulation**

In each grid cell, among the 100 bins, the bins that the long-term WTD has ever been shallower than 25cm are classified as ‘potential peatlands’, which are used for peatland simulation (Figure 1 (b)). To be consistent with the WTD simulation, long-term WTD refers to the 50-year moving average of annual WTD. In this study, we assume within each grid cell, the climate conditions are similar and the key control of whether peat exists at sub-grid cell scale is the local WTD influenced by sub-grid topography. Therefore, for all the bins in the same 0.5°×0.5° grid cell, the forcing data, soil texture, elevation and parameters are the same except for the input WTD.

In Holocene simulations, the maximum C assimilated by ecosystem parameter ($c_{max}$) is calibrated for over 2000 peat cores and interpolated into the pan-Arctic region (Zhao et al., 2022a). The calibration process reduces the uncertainty from forcing data, other parameters and model structure, and the simulated spatial and temporal pattern of pan-Arctic peatland C stock is consistent with multiple datasets (Zhao et al., 2022a). However, since the hydrology module of PTEM 2.2 is revised and peat accumulation and decomposition is sensitive to hydrological processes, using the original parameters could result in considerable bias. In order to make sure the revised PTEM 2.2 simulates consistent C accumulation rate (CAR) with the previous study, a spatially explicit calibration on maximum C assimilated by ecosystem ($c_{max}$) parameter is conducted.

https://doi.org/10.5194/egusphere-2022-1006
Preprint. Discussion started: 30 September 2022


Before calibrating CAR, it is necessary to initialize PTEM 2.2 with reasonable peat conditions. To initialize the simulation, the peat profile in 1940 derived from the Holocene simulation (Zhao et al., 2022a) is used (Figure 1 (b)). In particular, the peat profile records the physical property of vertical peat layers including bulk density, organic C density, layer thickness (1cm except for the top layer), fraction of remaining undecomposed organic matter and decomposition rate of undecomposed organic matter at 0°C. This information can be used to estimate the decomposition rate of existing peat given WTD, soil pH and soil temperature (Zhao et al., 2022b).

With initial peat profile as an input, $c_{max}$ values are calibrated with PEST (v17.2 for Linux) (Figure 1 (b)). In particular, within each grid cell, the 50-year average CAR of historical wetland bins (i.e., the bins that are classified as wetlands during 1940-1990) are simulated and averaged to get the grid cell average 50-year peatland CAR. This grid cell average peatland CAR is calibrated against the CAR derived from the Holocene simulation during the same period (SI Figure 5).

After calibration, the peat simulation is conducted for all pan-Arctic potential peatland bins during 1940-2300 (Figure 1 (b)). For the Greenland grid cells not included in the Holocene simulation and thereby have no calibrated $c_{max}$ values, the $c_{max}$ values are interpolated from adjacent grid cells. For the bins not included in the Holocene simulation or not being peatlands before 1990, the peat profile is initialized as 3cm fully decomposed peat. Notably, under different forcing data and warming scenarios, the number and distribution of potential peatland bins are slightly different, which makes the initial pan-Arctic peatland C storage in 1940 slightly different (SI Table 1). When running peat simulation, the forcing input (temperature, precipitation, cloudiness and vapor pressure), soil texture, elevation and parameters are the same as the ones used in the WTD simulation, except for the spatial-explicit $c_{max}$ values.

### 2.3.3. Peat simulation post-processing

After simulation, the simulated results are analyzed in terms of 1) the temporal pattern of pan-Arctic climate dynamics; 2) the temporal pattern of pan-Arctic peatland C stocks and C fluxes; 3) the main drivers of pan-Arctic peatland C dynamics; and 4) the threshold temperature and precipitation of pan-Arctic C sink/source shift.

Threshold temperature is calculated with logistic regression:

$$f(temp) = \begin{cases} 0 & NEP \leq 0 \\ 1 & NEP > 0 \end{cases} \tag{15}$$

Where NEP is net ecosystem productivity. A fitting curve of $f(temp)$ is derived for the pan-Arctic region and for each grid cell. Under sink-source shift, the fitting curve rises from 0 to 1, and the threshold temperature of sink-source shift is determined when $f(temp)$ is 0.5. The threshold precipitation is calculated in the same way.

## 3. Results

### 3.1 Warmer and drier pan-Arctic peatlands during 1990-2300

https://doi.org/10.5194/egusphere-2022-1006
Preprint. Discussion started: 30 September 2022


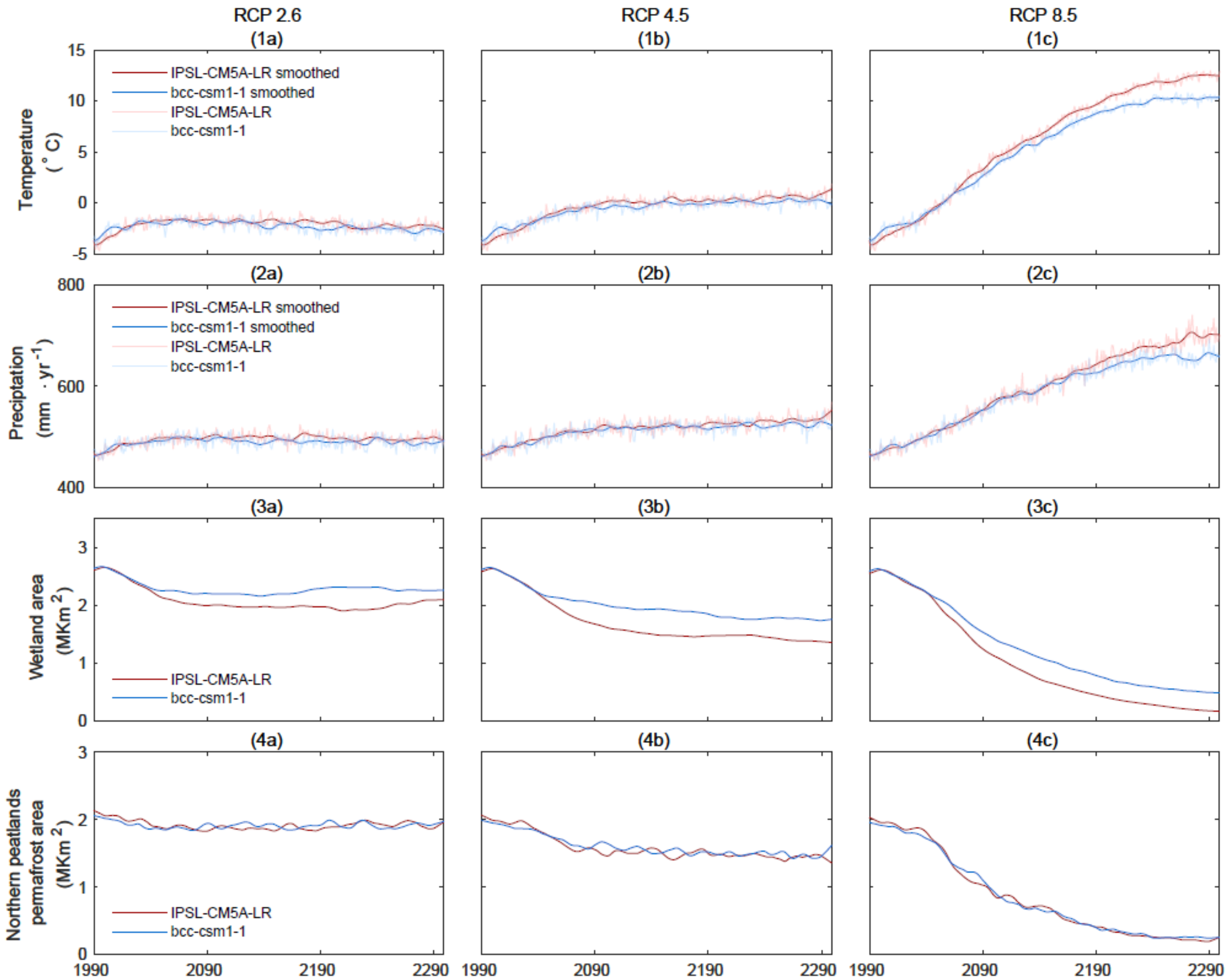


**Figure 2. Time series of pan-Arctic annual air temperature (°C), annual precipitation (mm·yr$^{-1}$), wetland area (Mkm$^2$) and permafrost area in peatland regions (Mkm$^2$) during 1990-2300.**

Both IPSL-CM5A-LR and bcc-csm1-1 climates show higher temperature and precipitation during 1990-2300. In particular, under RCP 2.6 and RCP 4.5, temperature increases mostly before 2100 by 2.3-4.1°C and 2.0-3.2°C under IPSL-CM5A-LR and bcc-csm1-1, respectively (Figure 2 1(a-b), SI Table 2). Meanwhile, precipitation increases by 40.7-59.7 mm·yr$^{-1}$ and 38.1-53.9 mm·yr$^{-1}$ for under IPSL-CM5A-LR and bcc-csm1-1 (Figure 2 2(a-b), SI Table 2). During 2100-2300, under RCP 2.6, the temperature decreases by 0.8°C in IPSL-CM5A-LR and by 1.1°C in bcc-csm1-1. Under RCP 4.5, temperature keeps increasing but in a slower rate than before 2100 (IPSL-CM5A-LR: 1.3°C vs. bcc-csm1-1: 0.4°C). Meanwhile, precipitation slightly decreases under RCP 2.6 (IPSL-CM5A-LR: -12.0 mm·yr$^{-1}$ vs. bcc-csm1-1: -5.8 mm·yr$^{-1}$) while increases under RCP 4.5 (IPSL-CM5A-LR: 29.1 mm·yr$^{-1}$ vs. bcc-csm1-1: 8.5 mm·yr$^{-1}$) (Figure 2 1(a-b) &2(a-b), SI Table 2). Different from RCP 2.6 and RCP 4.5, the increase in temperature and precipitation under RCP 8.5 is stable throughout 1990-2300. In particular, under IPSL-CM5A-LR, during 1990-2100 and 2100-2300, temperature increases by 8.4

and 8.1 °C while precipitation increases by 106.1 and 131.7 mm·$yr^{-1}$. Under bcc-csm1-1, during 1990-2100 and 2100-2300, temperature increases by 7.2 and 6.9 °C while precipitation increases by 100.9 and 198 mm·$yr^{-1}$, respectively (Figure 2 (1-2)c, SI Table 2).

The result of pan-Arctic wetland shrinking under all scenarios indicates that the increase of precipitation does not compensate the increase of evapotranspiration under warmer climate. Therefore, the pan-Arctic generally becomes drier and WTD becomes deeper (Figure 2 3(a-c)). In particular, during 1990-2100, under IPSL-CM5A-LR, wetland shrinks by 0.6, 0.9 and 1.4 million $km^2$ under three RCP scenarios. Meanwhile, under bcc-csm1-1, wetland shrinks slightly less by 0.4, 0.6 and 1.2 million $km^2$ under three RCP scenarios, respectively. During 2100-2300, under both IPSL-CM5A-LR and bcc-csm1-1, wetlands slightly expand by 0.1 million $km^2$ under RCP 2.6, while under the warmer scenarios, wetland further shrinks by 0.2 and 0.9 million $km^2$, respectively (Figure 2 3(a-c), SI Table 2).

Following climate warming, permafrost shrink is simulated across the current pan-Arctic peatland region under all scenarios (Figure 2 4(a-c)). In particular, with IPSL-CM5A-LR forcing, under RCP 2.6, 4.5 and 8.5, permafrost shrinks by 0.2, 0.7 and 1.2 million $km^2$ during 1990-2100 and expands by 0.1, shrinks by 0.1 and 0.5 million $km^2$, respectively, during 2100-2300. Meanwhile, active layer deepening is simulated in the remaining permafrost region (SI Figure 6). Similarly, with bcc-csm1-1 forcing, under RCP 2.6, 4.5 and 8.5, permafrost shrinks by 0.2, 0.2 and 1.0 million $km^2$ during 1990-2100 and expands by 0.1, shrinks by 0.1 and 0.6 million $km^2$, respectively, during 2100-2300 (Figure 2 4(a-c), SI Table 2). Meanwhile, active layer deepening is simulated in the remaining permafrost region under RCP 4.5 and 8.5 (SI Figure 7).

Under RCP 2.6 and 4.5, with both IPSL-CM5A-LR and bcc-csm1-1 forcing, peatlands (i.e., the region with peat thickness >= 30cm) area expands during 1990-2300 (Figure 3). In particular, the new peat area expands by 0.1 to 0.2 million $km^2$, while the old peat area is stable (SI Table 2). Under RCP 8.5, however, peatland area shrinks. In particular, although new peat land area expands by 0.1 million $km^2$, the old peatland area shrinks by 0.1 to 0.4 million $km^2$, causing total peatland area decrease (Figure 3, SI Table 2).

https://doi.org/10.5194/egusphere-2022-1006
Preprint. Discussion started: 30 September 2022


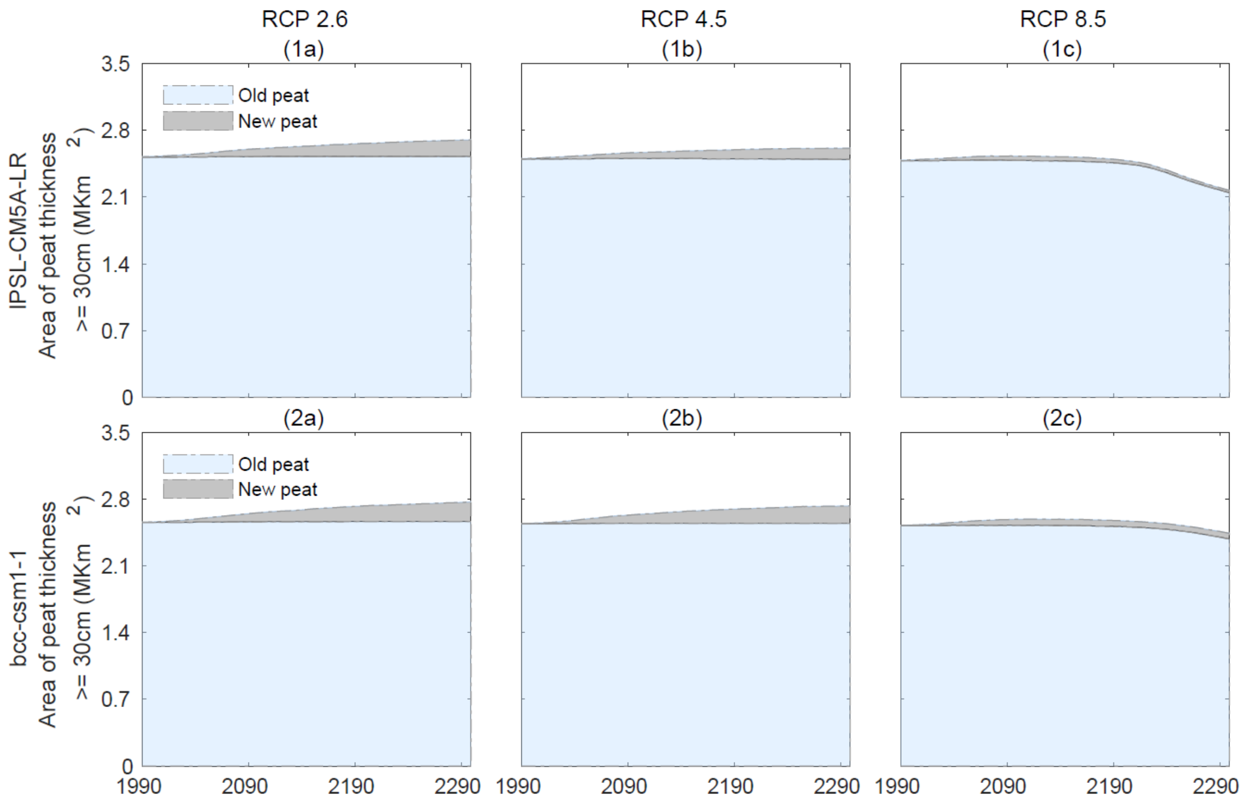


**Figure 3. Time series of pan-Arctic old and new peatland area (million km$^2$) during 1990-2300.**

## 3.2 Pan-Arctic C stocks and fluxes under climate change

### 3.2.1 Before 2100

With WTD becomes deeper, active layer depth (ALD) becomes deeper and permafrost extent shrink, it is reasonable that decomposition increases during 1990-2100 under all scenarios (Figure 4 3&4 (a-c), SI Table 3). Meanwhile, NPP slightly decreases with IPSL-CM5A-LR forcing while increases with bcc-csm1-1 forcing (Figure 4 2(a-c), SI Table 3). In PTEM 2.2, NPP is primarily influenced by temperature and nitrogen availability, and available nitrogen mainly comes from net N mineralization. In all scenarios, net N mineralization rate increases (negative values indicate higher net N mineralization) during 1990-2100 (SI Figure 8), indicating more available N for vegetation. The increase in both N availability and temperature can not explain the reason for NPP decrease. However, NPP decrease can be explained by the shift in PFTs. In particular, during 1990-2100, with water table becomes deeper, the dominance of herbaceous plants is gradually replaced by woody plants (i.e., shrubs and trees) that can thrive under drier conditions (SI Figure 9). In PTEM 2.2, compared with herbaceous plants, woody plants require more nitrogen for production. Therefore, although N availability increases, the increase is not sufficient for woody plants to maintain as high NPP as herbaceous plants and the overall NPP decreases.

https://doi.org/10.5194/egusphere-2022-1006
Preprint. Discussion started: 30 September 2022


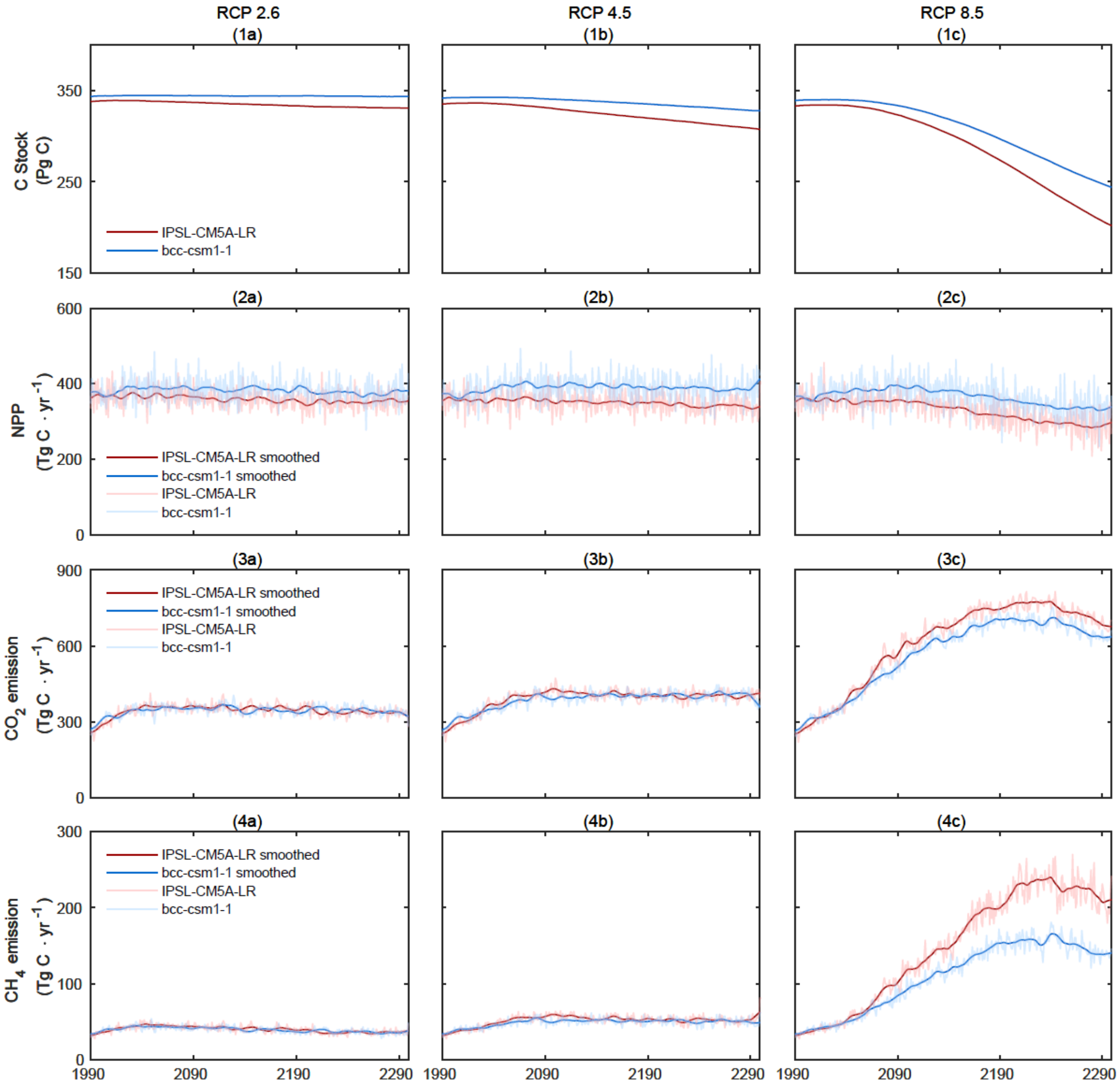


**Figure 4. Time series of pan-Arctic peatland C storage (vegetation and soil, Pg C), NPP ($TgC\cdot yr^{-1}$), $CO_2$ emissions ($TgC\cdot yr^{-1}$) and $CH_4$ emissions ($TgC\cdot yr^{-1}$) during 1990-2300.**

In all scenarios except for bcc-csm1-1 RCP 2.6, the increase in decomposition overrides the increase in NPP and thereby C stock decreases (Figure 4 1(a-c), SI Table 3). In particular, with ISP-CM5A-LR forcing, by 2100, C stock decreases by 1.3, 5.2 and 13.3 Pg C under RCP 2.6, 4.5 and 8.5, respectively. With bcc-csm1-1 forcing, by 2100, C stock increases by 0.8 Pg C under RCP 2.6, while decreases by 1.2 and 7.8 Pg C under RCP 4.5 and 8.5, respectively (Figure 4 1(a-c), SI Table 3). Notably, although pan-Arctic peatlands are C sinks during 1990-2100 under bcc-csm1-1 RCP 2.6, the

https://doi.org/10.5194/egusphere-2022-1006
Preprint. Discussion started: 30 September 2022


sink is much lower than that during 1940-1990 with CAR decreases by 29.1 $gC\cdot m^{-2}\cdot yr^{-1}$. Furthermore, this difference is larger in the other scenarios (IPSL-CM5A-LR: 35.5-63.5 $gC\cdot m^{-2}\cdot yr^{-1}$, bcc-csm1-1: 34.6-50.0 $gC\cdot m^{-2}\cdot yr^{-1}$) (SI Figure 10&11, SI Table 4).

**3.2.2 During 2100-2300**

During 2100-2300, the decrease in decomposition rate is simulated in RCP 2.6 and 4.5 with both forcing, while decomposition rate becomes higher under RCP 8.5 (SI Table 3). Under RCP 2.6, the decrease in decomposition is driven by the colder and wetter climate (Figure 2), while with IPSL-CM5A-LR forcing the decrease of C stock also influences decomposition rate negatively. In contrast, under RCP 4.5 where climate becomes warmer and drier, the decrease in decomposition rate is mostly driven by the lower C stock available for decomposition. However, under RCP 8.5 where the climate change is more severe, the positive effect of warming and drying overrides the negative effect of insufficient C stock and thereby decomposition rate keeps increasing (Figure 4 3&4(a-c), SI Table 3).

During 2100-2300, NPP in all scenarios decrease except for bcc-csm1-1 RCP 4.5 (Figure 4 2(a-b), SI Table 3). For both forcings, under RCP 2.6 and 4.5, PFT distribution is stable after 2100 (SI Figure 9 1&2(a-b)). Therefore, NPP is driven by the balance of net N mineralization and temperature. For bcc-csm1-1 RCP 4.5, the positive effect of temperature overrides the negative effect of decreasing net N mineralization, while the opposite is found in the other scenarios (SI Figure 8). Under RCP 8.5, with further herbaceous-woody switch and decrease in net N mineralization, NPP decreases with both forcings (Figure 4 2(c), SI Table 3). With NPP decrease and decomposition increase, pan-Arctic peatlands are C sources under all scenarios. In particular, with IPSL-CM5A-LR forcing, under RCP 2.6, 4.5 and 8.5, pan-Arctic peatlands are sources of 5.9, 22.5 and 118.3 Pg C, respectively, while these values are 0.7, 12.6 and 87.6 Pg C with bcc-csm1-1 forcing, respectively (Figure 4 1(a-c), SI Table 3). During 2100-2300, CAR is lower than that during the 21st century. In particular, under RCP 2.6, 4.5 and 8.5, CAR further decreases by 4.6-9.3 $gC\cdot m^{-2}\cdot yr^{-1}$, 23.9-25.7 $gC\cdot m^{-2}\cdot yr^{-1}$ and 135.5-193.8 $gC\cdot m^{-2}\cdot yr^{-1}$ with IPSL-CM5A-LR forcing and 4.1-4.9 $gC\cdot m^{-2}\cdot yr^{-1}$, 15.7-20.6 $gC\cdot m^{-2}\cdot yr^{-1}$ and 103.7-145.3 $gC\cdot m^{-2}\cdot yr^{-1}$ with bcc-csm1-1 forcing, respectively (SI Figure 10&11, SI Table 4).

**3.3 Pan-Arctic peatlands C sinks in response to climate change**

For both IPSL-CM5A-LR and bcc-csm1-1 forcings, the positive correlation between temperature and precipitation is found at the pan-Arctic scale (Table 1). In particular, with 1°C annual temperature increase, the annual precipitation increases by 13.84-15.33 $mm\cdot yr^{-1}$ in IPSL-CM5A-LR forcing and 13.78-14.59 $mm\cdot yr^{-1}$ in bcc-csm1-1 forcing. The correlation has higher $R^2$ values in warmer scenarios. The positive correlation between temperature and precipitation is mostly found in Eurasia and northeast America, where the $R^2$ values are also higher than the other region (SI Figure 12&13).

The negative correlation between temperature and pan-Arctic peatland C sink activity is found in both forcing scenarios (Table 1). In particular, with 1°C annual temperature increase, pan-Arctic peatland C sink decreases by 40.46-46.91 $Tg\ C\cdot yr^{-1}$ in IPSL-CM5A-LR forcing and 33.27-41.1 $Tg\ C\cdot yr^{-1}$ in bcc-csm1-1 forcing. The negative effect of temperature is weaker in western Eurasia and Alaska regions, while stronger in the other regions where most of the current peatlands exist (SI Figure 14&15). Due to the close positive correlation between temperature and precipitation, the

https://doi.org/10.5194/egusphere-2022-1006
Preprint. Discussion started: 30 September 2022


correlation between precipitation and pan-Arctic peatland C sink is also negative. In particular, with 1mm annual precipitation increase, pan-Arctic peatland C sink decreases by 2.32-3.28 Tg C·yr$^{-1}$ in IPSL-CM5A-LR forcing and 1.85-2.92 Tg C·yr$^{-1}$ in bcc-csm1-1 forcing (Table 1). The spatial pattern of precipitation-C sink correlation is consistent with the spatial pattern of temperature-C sink correlation (SI Figure 16&17).

At the pan-Arctic scale, a threshold annual temperature and precipitation can be found when peatlands switch from a C sink to a source. In particular, with IPSL-CM5A-LR forcing, the threshold annual temperature is -2.89 - -2.6°C and the threshold precipitation is 479.59 - 482.55 mm. With bcc-csm1-1 forcing, the threshold annual temperature is -2.35 - -2.09°C and the threshold precipitation is 484.69 - 489.02 mm (Table 1). The threshold temperature varies spatially with mostly below -3°C in the northern North American and western Eurasia regions and mostly above 1°C in the lower latitude regions (SI Figure 18). Notably, the regions with below -3°C threshold temperature tend to have higher $R^2$ values (SI Figure 19). The spatial pattern of precipitation threshold is consistent with temperature threshold and the region with 300-500mm annual precipitation threshold has higher $R^2$ values, mostly seen in northern North American and western Eurasia (SI Figure 20&21).

**Table 1.** Relationship between pan-Arctic temperature, precipitation and C sink

| Model | RCP 2.6 | $R^2$ | RCP 4.5 | $R^2$ | RCP 8.5 | $R^2$ |
|---|---|---|---|---|---|---|
| Pan-Arctic peatlands C sink capability increases (TgC·yr$^{-1}$) in response to 1°C annual temperature increase | | | | | | |
| IPSL-CM5A-LR | -43.92 | 0.72 | -40.46 | 0.86 | -46.91 | 0.96 |
| bcc-csm1-1 | -34.59 | 0.51 | -33.27 | 0.76 | -41.1 | 0.96 |
| Pan-Arctic peatlands C sink capability increases (TgC·yr$^{-1}$) in response to 1mm annual precipitation increase | | | | | | |
| IPSL-CM5A-LR | -2.32 | 0.64 | -2.47 | 0.78 | -3.28 | 0.92 |
| bcc-csm1-1 | -1.85 | 0.46 | -2.06 | 0.73 | -2.92 | 0.94 |
| Annual temperature threshold of C sink-source conversion | | | | | | |
| IPSL-CM5A-LR | -2.89 | 0.57 | -2.72 | 0.9 | -2.6 | 0.86 |
| bcc-csm1-1 | -2.35 | 0.16 | -2.12 | 0.64 | -2.09 | 0.81 |
| Annual precipitation threshold of C sink-source conversion | | | | | | |
| IPSL-CM5A-LR | 479.59 | 0.51 | 482.42 | 0.86 | 482.55 | 0.84 |
| bcc-csm1-1 | 489.02 | 0.16 | 485.5 | 0.63 | 484.69 | 0.79 |
| Annual precipitation increase (mm) in response to 1°C annual temperature increase | | | | | | |
| IPSL-CM5A-LR | 15.33 | 0.74 | 14.71 | 0.9 | 13.84 | 0.98 |
| bcc-csm1-1 | 13.78 | 0.61 | 14.59 | 0.85 | 13.78 | 0.98 |

## 4. Discussion

### 4.1 Wetlands and permafrost dynamics under climate change

https://doi.org/10.5194/egusphere-2022-1006
Preprint. Discussion started: 30 September 2022


Wetlands loss is closely related to climate change and human activities. In particular, the loss has been found globally since 1700AD, with 64-71% loss since 1900 AD (Davidson, 2014). Similarly, a more recent study has found 33% of the global wetland loss as of 2009, with 45% in Europe and 8% in North America (Hu et al., 2017). In addition, regional studies also report different scales of wetlands loss in China and coastal regions (Li et al., 2018; Niu et al., 2012). To date, no many studies focus on future wetland extent simulations and the inconsistency among current wetland extent datasets exists (Loveland et al., 2000; Friedl et al., 2002; Lehner and Döll, 2004; Bartholomé and Belward, 2005). Similar to this study, one study highlighted the vulnerability of Arctic wetland extent in the 21st century due to permafrost thaw, although most of the permafrost Arctic wetlands can remain stable under RCP 2.6 until at least 2100 (Kåresdotter et al., 2021).

The active layer depth (ALD) simulated by PTEM 2.2 is compared with two datasets derived from satellite data and models, covering pan-Arctic region and Alaska, respectively (Obu et al., 2020; Yi and Kimball, 2020). The correlation with pan-Arctic dataset (2001-2018) is higher than the correlation with Alaska dataset, while the overall estimation is consistent between our study and two regional datasets (SI Table 3&4). Consistent with our study, Smith et al. (2022) found deepening ALD since the 1990s in the permafrost region, indicating permafrost thaw could continue in warmer future and possibly in a higher rate. The permafrost thaw progress in the 21$^{st}$ century agrees with the dynamics simulated by CCSM4 model, suggesting that the CCSM4 permafrost area shrinks by 64% by 2100 under RCP 8.5 compared to our estimation of 53-60% in this study (Lawrence et al., 2012).

**4.2 Future productivity and decomposition in northern peatlands**

In this study, NPP does not always increase under warmer climate due to PFT switch and net N mineralization rate limiting. The overall trend of pan-Arctic peatland PFT switch is the expansion of woody plants and shrink of herbaceous plants (SI Figure 9). A previous study found that peatland WTD deepening benefits shrub dominance while suppresses forbs and mosses (Mäkiranta et al., 2018). Meanwhile, shrub expansion is reported in Alaska, Siberian and across the pan-Arctic region under historical climate warming (Tape et al., 2006; Blok et al., 2010). Furthermore, the simulation based on LPJ-GUESS also predicts higher proportion of shrub NPP in lower latitude regions due to high insolation and deep WTD (Chaudhary et al., 2020). These studies support our findings that the future warmer and drier condition is the driver for PFT switch and benefits woody plants.

In PTEM 2.2, the net N mineralization rate is related to soil moisture (Zhao et al., 2022b). Therefore, whether future peatlands become more nutrient rich depending on the balance between the positive effect of higher temperature and the negative effect of lower soil moisture. The negative effect of drier soil overwhelms the influence of temperature and thereby net N mineralization rate decrease under RCP 8.5 after 2100 (SI Figure 8). Under a N limiting condition, the modeling study with LPX-Bern 1.0 found peatlands switch from a C sink to a source under RCP 8.5 with slow NPP increase, which is consistent with our simulation with bcc-csm1-1 forcing (Spahni et al., 2013).

Warming affects decomposition mainly in three ways. First, there is higher decomposition rate due to the lower WTD under warming climate conditions (Huang et al., 2021). Second, higher temperature also enhances decomposition more than productivity (Tang et al., 2022). Third, in high latitude regions, soil C decomposition rate is likely to increase under warmer climate and permafrost thaw conditions (Yokohata et al., 2020; Schneider Von Deimling et al., 2015; Gasser et al., 2018; Macdougall and Knutti, 2016; Schuur et al., 2015). In the warming future, the estimation of $CO_2$ release under RCP 2.6 tends to be higher than the values estimated from other models (by 2100: 54.7-54.8 Pg C in this study vs. 20-58 Pg C in literature; by 2300: 131.2-131.3 Pg C in this study vs. 40-98 Pg C in literature, Table 2). However, the estimation under RCP 8.5 is closer (by 2100: 55.2-57.2 Pg C in this study vs. 42-141 Pg C in literature; by 2300: 222.2-247.6 Pg C in this study vs. 157-313 Pg C in literature) (Yokohata et al., 2020; Schneider Von Deimling et al., 2015; Gasser et al., 2018) (Table 2). The $CH_4$ emission estimation is also higher than that in Yokohata (2020) by 5-6 Pg C by 2100, while the total C emission is close to the estimation of MacDougall (2016) (55 Pg C vs. 56 Pg C).

**4.3 Northern peatland C sink and source shift**

Our estimated CAR during 1990-2000 is 19.17-22.73 $gC·m^{-2}·yr^{-1}$, which is lower than that by Chaudhary et al. (2020) during the same period (33.9 $gC·m^{-2}·yr^{-1}$). However, our estimated CAR is closer to the core-based Holocene CAR (18.6-22.9 $gC·m^{-2}·yr^{-1}$) (Yu et al., 2009; Loisel et al., 2014). In this study, the estimated pan-Arctic peatlands annual $CH_4$ emissions are 28.7 Tg $C·yr^{-1}$ during 1990-2000, 33.0 Tg $C·yr^{-1}$ during 1990-2000 and 38.5 Tg $C·yr^{-1}$ during 2000-2020. The estimation after 1990 is close to the 36.0 Tg $C·yr^{-1}$ in Kleinen et al. (2020) while larger than 25.0 Tg $C·yr^{-1}$ reconstructed from historical data (Treat et al., 2021). However, the difference between our study and Treat et al. (2021) might result from different peatland coverages used in two studies. Under the peatland coverage of Nichols and Peteet (2019), the CH4 emissions in Treat et al. (2021) were 32.3-43.5 Tg $C·yr^{-1}$, which agrees better with our estimates.

Multiple studies have indicated there is a C loss trend of northern ecosystems under warming climate (Hanson et al., 2020; Piao et al., 2008; Helbig et al., 2017). In particular, the peatland experiment in Minnesota, USA suggests that warming increases C loss rate by 31.3 $gC·m^{-2}·yr^{-1}$ (Hanson et al., 2020). Similarly, another site-level study on Canadian boreal-wetland biome shows a decline of $CO_2$ uptake from 25±14 $gC·m^{-2}·yr^{-1}$ to 103±38 $gC·m^{-2}·yr^{-1}$ by 2100 depending on the warming scenarios (Helbig et al., 2017). These studies are consistent with our estimates, suggesting that northern peatlands CAR during 1990-2100 is lower than that during 1940-1990 by 29.1-63.5 $gC·m^{-2}·yr^{-1}$.

At the regional scale, whether northern peatlands will switch from a C sink to C source is still uncertain. For example, Gallego-Sala et al. (2018) indicates northern peatlands are likely to sequester more C under RCP 2.6 and RCP 8.5 until 2100. Chaudhary et al. (2020), however, indicates the C sink capacity of northern peatlands will decreases under RCP 8.5 after 2050. Similarly, McGuire et al. (2018) suggests northern permafrost region could be C sources after 2100 unless under aggressive climate change mitigation pathways. Furthermore, Qiu et al. (2022) simulates northern peatlands dynamics until 2300, suggesting a sink-source shift under RCP 8.5 while no such shift under RCP 2.6. Although conclusions vary among studies, they generally suggest a higher C source possibility under warmer scenarios, which agrees with the negative correlation between temperature and C sink capacity from this study. Furthermore, the arguments that northern peatlands keep being C sinks under RCP 2.6 (Gallego-Sala et al., 2018; Qiu et al., 2022) is consistent with our study under bcc-csm1-1 forcing. However, different from previous works (Gallego-Sala et al., 2018; Qiu et al., 2022; McGuire et al., 2018; Chaudhary et al., 2020), our study predicts northern peatlands to be C sources under RCP 2.6 before 2100 with IPSL-CM5A-

LR forcing. In addition, the C sink-source switch will occur before 2100 under RCP 4.5 and RCP 8.5. Except for the future decomposition increase, which is common among model predictions (Yokohata et al., 2020; Schneider Von Deimling et al., 2015; Gasser et al., 2018; Macdougall and Knutti, 2016; Schuur et al., 2015), these differences are mainly due to the suppressed NPP in this study.

## 5. Conclusions

Northern peatlands responses to future climate change during 1990-2300 are simulated with PTEM. The peatlands shrink or expansion, peat accumulation and decomposition processes are considered. Two sets of CMIP5 forcing data (IPSL-CM5A-LR and bcc-csm1-1) are used to drive the model with three warming scenarios (RCP 2.6, RCP 4.5 and RCP 8.5). We found that wetlands will shrink and permafrost will thaw under all scenarios, indicating pan-Arctic peatlands become warmer and drier. Northern peatland area expands under RCP 2.6 and RCP 4.5 while shrinks under RCP 8.5 due to high decomposition rate. NPP does not always increase with temperature because of PFT switch and N limiting effects. However, both $CO_2$ and $CH_4$ emissions increase with temperature due to lower WTD, thawing permafrost and higher temperature. By 2100, northern peatlands will be a minor C sink of 0.8 Pg C under RCP 2.6 with bcc-csm1-1 forcing while C sources under other scenarios. During 2100-2300, northern peatlands are C sources under all scenarios, the warmer climate results in the larger C source. There are negative correlations between temperature and northern peatland C sink under all scenarios. The negative correlation between precipitation and northern peatland C sink is also found under all scenarios, while this is likely due to the positive correlation between temperature and precipitation. When pan-Arctic annual temperature is -2.89 - -2.6°C with IPSL-CM5A-LR forcing or -2.35 - -2.09°C with bcc-csm1-1 forcing, the northern peatlands switch from a C sink to a source. Similarly, this threshold for annual precipitation is 479.59 - 482.55 mm with IPSL-CM5A-LR forcing and 484.69 - 489.02 mm with bcc-csm1-1 forcing. Our study highlights the current northern peatlands C sink might shift to a source under future warming and drying climate conditions.

## Acknowledgments

This study is financially supported by an NSF project (1802832).

## Coda and data availability:

The data used to reproduce figures in both text and supplementary material, PTEM 2.2 codes, model and samples of running directory can be accessed via Purdue University Research Repository: https://purr.purdue.edu/publications/4139/1.

## References

Allen, M. R., Dube, O. P., Solecki, W., Aragón-Durand, F., W. Cramer, S. H., Kainuma, M., J. Kala, N. M., Mulugetta, Y., Perez, R., Wairiu, M., and Zickfeld, K.: Framing and Context. In: Global Warming of 1.5°C. An IPCC Special Report on the impacts of global warming of 1.5°C above pre-industrial levels and related global greenhouse gas emission pathways, in the context of strengthening the global response to the threat of climate change, sustainable evelopment, and efforts to eradicate poverty, IPCC, 2018.

Allen, R. G., Pereira, L. S., Raes, D., and Smith, M.: Crop evapotranspiration - Guidelines for computing crop water requirements - FAO Irrigation and drainage paper 56, 1998.

Bartholomé, E. and Belward, A. S.: GLC2000: a new approach to global land cover mapping from Earth observation data, International Journal of Remote Sensing, 26, 1959-1977, 10.1080/01431160412331291297, 2005.
Beven, K. J. and Kirkby, M. J.: A physically based, variable contributing area model of basin hydrology / Un modèle à base physique de zone d'appel variable de l'hydrologie du bassin versant, Hydrological Sciences Bulletin, 24, 43-69, 10.1080/02626667909491834, 1979.
Blok, D., Heijmans, M. M. P. D., Schaepman-Strub, G., Kononov, A. V., Maximov, T. C., and Berendse, F.: Shrub expansion may reduce summer permafrost thaw in Siberian tundra, Global Change Biology, 16, 1296-1305, https://doi.org/10.1111/j.1365-2486.2009.02110.x, 2010.
Bohn, T. J., Podest, E., Schroeder, R., Pinto, N., McDonald, K. C., Glagolev, M., Filippov, I., Maksyutov, S., Heimann, M., Chen, X., and Lettenmaier, D. P.: Modeling the large-scale effects of surface moisture heterogeneity on wetland carbon fluxes in the West Siberian Lowland, Biogeosciences, 10, 6559-6576, 10.5194/bg-10-6559-2013, 2013.
Brooks, R. H.: HYDRAULIC PROPERTIES OF POROUS MEDIA, Ph.D., Colorado State University, Ann Arbor, 101 pp., 1965.
Carter, A. J. and Scholes, R. J.: SoilData v2.0: Generating a Global Database of Soil Properties CSIR Environmentek, Pretoria, South Africa, 2000.
Chaudhary, N., Miller, P. A., and Smith, B.: Modelling past, present and future peatland carbon accumulation across the pan-Arctic region, Biogeosciences, 14, 4023-4044, 10.5194/bg-14-4023-2017, 2017.
Chaudhary, N., Westermann, S., Lamba, S., Shurpali, N., Sannel, A. B. K., Schurgers, G., Miller, P. A., and Smith, B.: Modelling past and future peatland carbon dynamics across the pan-Arctic, Global Change Biology, n/a, 10.1111/gcb.15099, 2020.
Davidson, N. C.: How much wetland has the world lost? Long-term and recent trends in global wetland area, Marine and Freshwater Research, 65, 934-941, https://doi.org/10.1071/MF14173, 2014.
Fan, Y., Li, H., and Miguez-Macho, G.: Global Patterns of Groundwater Table Depth, Science, 339, 940, 10.1126/science.1229881, 2013.
FAO/UNESCO: Soil Map of the World, Food and Agriculture Organization of the United Nations, Paris, 1974.
Finger Higgens, R. A., Chipman, J. W., Lutz, D. A., Culler, L. E., Virginia, R. A., and Ogden, L. A.: Changing Lake Dynamics Indicate a Drier Arctic in Western Greenland, Journal of Geophysical Research: Biogeosciences, 124, 870-883, https://doi.org/10.1029/2018JG004879, 2019.
Finlayson, C. M. and Milton, G. R.: Peatlands, in: The Wetland Book: II: Distribution, Description, and Conservation, edited by: Finlayson, C. M., Milton, G. R., Prentice, R. C., and Davidson, N. C., Springer Netherlands, Dordrecht, 227-244, 10.1007/978-94-007-4001-3_202, 2018.
Franchini, M. and Pacciani, M.: Comparative analysis of several conceptual rainfall-runoff models, Journal of Hydrology, 122, 161-219, https://doi.org/10.1016/0022-1694(91)90178-K, 1991.
Friedl, M. A., McIver, D. K., Hodges, J. C. F., Zhang, X. Y., Muchoney, D., Strahler, A. H., Woodcock, C. E., Gopal, S., Schneider, A., Cooper, A., Baccini, A., Gao, F., and Schaaf, C.: Global land cover mapping from MODIS: algorithms and early results, Remote Sensing of Environment, 83, 287-302, https://doi.org/10.1016/S0034-4257(02)00078-0, 2002.
Gallego-Sala, A. V., Charman, D. J., Brewer, S., Page, S. E., Prentice, I. C., Friedlingstein, P., Moreton, S., Amesbury, M. J., Beilman, D. W., Björck, S., Blyakharchuk, T., Bochicchio, C., Booth, R. K., Bunbury, J., Camill, P., Carless, D., Chimner, R. A., Clifford, M., Cressey, E., Courtney-Mustaphi, C., De Vleeschouwer, F., de Jong, R., Fialkiewicz-Koziel, B., Finkelstein, S. A., Garneau, M., Githumbi, E., Hribjlan, J., Holmquist, J., Hughes, P. D. M., Jones, C., Jones, M. C., Karofeld, E., Klein, E. S., Kokfelt, U., Korhola, A., Lacourse, T., Le Roux, G., Lamentowicz, M., Large, D., Lavoie, M., Loisel, J., Mackay, H., MacDonald, G. M., Makila, M., Magnan, G., Marchant, R., Marcisz, K., Martínez Cortizas, A., Massa, C., Mathijssen, P., Mauquoy, D., Mighall, T., Mitchell, F. J. G., Moss, P., Nichols, J., Oksanen, P. O., Orme, L., Packalen, M. S., Robinson, S., Roland, T. P., Sanderson, N. K., Sannel, A. B. K., Silva-Sánchez, N., Steinberg, N., Swindles, G. T., Turner, T. E., Uglow, J., Väliranta, M., van Bellen, S., van der Linden, M., van Geel, B., Wang, G., Yu, Z., Zaragoza-Castells, J., and Zhao, Y.: Latitudinal limits to the predicted increase of the peatland carbon sink with warming, Nature Climate Change, 8, 907-913, 10.1038/s41558-018-0271-1, 2018.
Gandois, L., Hoyt, A. M., Hatté, C., Jeanneau, L., Teisserenc, R., Liotaud, M., and Tananaev, N.: Contribution of Peatland Permafrost to Dissolved Organic Matter along a Thaw Gradient in North Siberia, Environmental Science & Technology, 53, 14165-14174, 10.1021/acs.est.9b03735, 2019.

Gasser, T., Kechiar, M., Ciais, P., Burke, E. J., Kleinen, T., Zhu, D., Huang, Y., Ekici, A., and Obersteiner, M.: Path-dependent reductions in CO2 emission budgets caused by permafrost carbon release, Nature Geoscience, 11, 830-835, 10.1038/s41561-018-0227-0, 2018.

Hamman, J. J., Nijssen, B., Bohn, T. J., Gergel, D. R., and Mao, Y.: The Variable Infiltration Capacity model version 5 (VIC-5): infrastructure improvements for new applications and reproducibility, Geosci. Model Dev., 11, 3481-3496, 10.5194/gmd-11-3481-2018, 2018.

Hanson, P. J., Griffiths, N. A., Iversen, C. M., Norby, R. J., Sebestyen, S. D., Phillips, J. R., Chanton, J. P., Kolka, R. K., Malhotra, A., Oleheiser, K. C., Warren, J. M., Shi, X., Yang, X., Mao, J., and Ricciuto, D. M.: Rapid Net Carbon Loss From a Whole-Ecosystem Warmed Peatland, AGU Advances, 1, e2020AV000163, https://doi.org/10.1029/2020AV000163, 2020.

Harris, I., Jones, P. D., Osborn, T. J., and Lister, D. H.: Updated high-resolution grids of monthly climatic observations – the CRU TS3.10 Dataset, International Journal of Climatology, 34, 623-642, https://doi.org/10.1002/joc.3711, 2014.

He, F.: SIMULATING TRANSIENT CLIMATE EVOLUTION OF THE LAST DEGLACIATION WITH CCSM3, Atmospheric and Oceanic Sciences, UNIVERSITY OF WISCONSIN-MADISON, Madison, 2011.

Helbig, M., Chasmer, L. E., Desai, A. R., Kljun, N., Quinton, W. L., and Sonnentag, O.: Direct and indirect climate change effects on carbon dioxide fluxes in a thawing boreal forest–wetland landscape, Global Change Biology, 23, 3231-3248, https://doi.org/10.1111/gcb.13638, 2017.

Hu, S., Niu, Z., Chen, Y., Li, L., and Zhang, H.: Global wetlands: Potential distribution, wetland loss, and status, Science of The Total Environment, 586, 319-327, https://doi.org/10.1016/j.scitotenv.2017.02.001, 2017.

Huang, Y., Ciais, P., Luo, Y., Zhu, D., Wang, Y., Qiu, C., Goll, D. S., Guenet, B., Makowski, D., De Graaf, I., Leifeld, J., Kwon, M. J., Hu, J., and Qu, L.: Tradeoff of CO2 and CH4 emissions from global peatlands under water-table drawdown, Nature Climate Change, 11, 618-622, 10.1038/s41558-021-01059-w, 2021.

Hugelius, G., Loisel, J., Chadburn, S., Jackson, R. B., Jones, M., MacDonald, G., Marushchak, M., Olefeldt, D., Packalen, M., Siewert, M. B., Treat, C., Turetsky, M., Voigt, C., and Yu, Z.: Large stocks of peatland carbon and nitrogen are vulnerable to permafrost thaw, Proceedings of the National Academy of Sciences, 117, 20438, 10.1073/pnas.1916387117, 2020.

Hugelius, G., Bockheim, J. G., Camill, P., Elberling, B., Grosse, G., Harden, J. W., Johnson, K., Jorgenson, T., Koven, C. D., Kuhry, P., Michaelson, G., Mishra, U., Palmtag, J., Ping, C. L., O'Donnell, J., Schirrmeister, L., Schuur, E. A. G., Sheng, Y., Smith, L. C., Strauss, J., and Yu, Z.: A new data set for estimating organic carbon storage to 3 m depth in soils of the northern circumpolar permafrost region, Earth Syst. Sci. Data, 5, 393-402, 10.5194/essd-5-393-2013, 2013.

Kåresdotter, E., Destouni, G., Ghajarnia, N., Hugelius, G., and Kalantari, Z.: Mapping the Vulnerability of Arctic Wetlands to Global Warming, Earth's Future, 9, e2020EF001858, https://doi.org/10.1029/2020EF001858, 2021.

Kleinen, T., Mikolajewicz, U., and Brovkin, V.: Terrestrial methane emissions from the Last Glacial Maximum to the preindustrial period, Clim. Past, 16, 575-595, 10.5194/cp-16-575-2020, 2020.

Lawrence, D. M., Slater, A. G., and Swenson, S. C.: Simulation of Present-Day and Future Permafrost and Seasonally Frozen Ground Conditions in CCSM4, Journal of Climate, 25, 2207-2225, 10.1175/JCLI-D-11-00334.1, 2012.

Lehner, B. and Döll, P.: Development and validation of a global database of lakes, reservoirs and wetlands, Journal of Hydrology, 296, 1-22, https://doi.org/10.1016/j.jhydrol.2004.03.028, 2004.

Li, X., Bellerby, R., Craft, C., and Widney, S. E.: Coastal wetland loss, consequences, and challenges for restoration, Anthropocene Coasts, 1, 1-15, 10.1139/anc-2017-0001, 2018.

Liang, X., Lettenmaier, D. P., Wood, E. F., and Burges, S. J.: A simple hydrologically based model of land surface water and energy fluxes for general circulation models, Journal of Geophysical Research: Atmospheres, 99, 14415-14428, https://doi.org/10.1029/94JD00483, 1994.

Liu, C., Sun, G., McNulty, S. G., Noormets, A., and Fang, Y.: Environmental controls on seasonal ecosystem evapotranspiration/potential evapotranspiration ratio as determined by the global eddy flux measurements, Hydrol. Earth Syst. Sci., 21, 311-322, 10.5194/hess-21-311-2017, 2017.

Loisel, J., Yu, Z., Beilman, D. W., Camill, P., Alm, J., Amesbury, M. J., Anderson, D., Andersson, S., Bochicchio, C., Barber, K., Belyea, L. R., Bunbury, J., Chambers, F. M., Charman, D. J., De Vleeschouwer, F., Fiałkiewicz-Kozieł, B., Finkelstein, S. A., Gałka, M., Garneau, M., Hammarlund, D., Hinchcliffe, W., Holmquist, J., Hughes, P., Jones, M. C., Klein, E. S., Kokfelt, U., Korhola, A., Kuhry, P., Lamarre, A., Lamentowicz, M., Large, D., Lavoie, M., MacDonald, G.,

https://doi.org/10.5194/egusphere-2022-1006
Preprint. Discussion started: 30 September 2022


Magnan, G., Mäkilä, M., Mallon, G., Mathijssen, P., Mauquoy, D., McCarroll, J., Moore, T. R., Nichols, J., O'Reilly, B., Oksanen, P., Packalen, M., Peteet, D., Richard, P. J. H., Robinson, S., Ronkainen, T., Rundgren, M., Sannel, A. B. K., Tarnocai, C., Thom, T., Tuittila, E.-S., Turetsky, M., Väliranta, M., van der Linden, M., van Geel, B., van Bellen, S., Vitt, D., Zhao, Y., and Zhou, W.: A database and synthesis of northern peatland soil properties and Holocene carbon and nitrogen accumulation, The Holocene, 24, 1028-1042, 10.1177/0959683614538073, 2014.

Loisel, J., Gallego-Sala, A. V., Amesbury, M. J., Magnan, G., Anshari, G., Beilman, D. W., Benavides, J. C., Blewett, J., Camill, P., Charman, D. J., Chawchai, S., Hedgpeth, A., Kleinen, T., Korhola, A., Large, D., Mansilla, C. A., Müller, J., van Bellen, S., West, J. B., Yu, Z., Bubier, J. L., Garneau, M., Moore, T., Sannel, A. B. K., Page, S., Väliranta, M., Bechtold, M., Brovkin, V., Cole, L. E. S., Chanton, J. P., Christensen, T. R., Davies, M. A., De Vleeschouwer, F., Finkelstein, S. A., Frolking, S., Gałka, M., Gandois, L., Girkin, N., Harris, L. I., Heinemeyer, A., Hoyt, A. M., Jones, M. C., Joos, F., Juutinen, S., Kaiser, K., Lacourse, T., Lamentowicz, M., Larmola, T., Leifeld, J., Lohila, A., Milner, A. M., Minkkinen, K., Moss, P., Naafs, B. D. A., Nichols, J., O'Donnell, J., Payne, R., Philben, M., Piilo, S., Quillet, A., Ratnayake, A. S., Roland, T. P., Sjögersten, S., Sonnentag, O., Swindles, G. T., Swinnen, W., Talbot, J., Treat, C., Valach, A. C., and Wu, J.: Expert assessment of future vulnerability of the global peatland carbon sink, Nature Climate Change, 11, 70-77, 10.1038/s41558-020-00944-0, 2021.

Loveland, T. R., Reed, B. C., Brown, J. F., Ohlen, D. O., Zhu, Z., Yang, L., and Merchant, J. W.: Development of a global land cover characteristics database and IGBP DISCover from 1 km AVHRR data, International Journal of Remote Sensing, 21, 1303-1330, 10.1080/014311600210191, 2000.

Lu, X. and Zhuang, Q.: Modeling methane emissions from the Alaskan Yukon River basin, 1986–2005, by coupling a large-scale hydrological model and a process-based methane model, Journal of Geophysical Research: Biogeosciences, 117, https://doi.org/10.1029/2011JG001843, 2012.

MacDougall, A. H. and Knutti, R.: Projecting the release of carbon from permafrost soils using a perturbed parameter ensemble modelling approach, Biogeosciences, 13, 2123-2136, 10.5194/bg-13-2123-2016, 2016.

Mäkiranta, P., Laiho, R., Mehtätalo, L., Straková, P., Sormunen, J., Minkkinen, K., Penttilä, T., Fritze, H., and Tuittila, E.: Responses of phenology and biomass production of boreal fens to climate warming under different water-table level regimes, Glob Chang Biol, 24, 944-956, doi: 10.1111/gcb.13934, 2018.

Marthews, T. R., Dadson, S. J., Lehner, B., Abele, S., and Gedney, N.: High-resolution global topographic index values for use in large-scale hydrological modelling, Hydrol. Earth Syst. Sci., 19, 91-104, 10.5194/hess-19-91-2015, 2015.

McGuire, A. D., Lawrence, D. M., Koven, C., Clein, J. S., Burke, E., Chen, G., Jafarov, E., MacDougall, A. H., Marchenko, S., Nicolsky, D., Peng, S., Rinke, A., Ciais, P., Gouttevin, I., Hayes, D. J., Ji, D., Krinner, G., Moore, J. C., Romanovsky, V., Schädel, C., Schaefer, K., Schuur, E. A. G., and Zhuang, Q.: Dependence of the evolution of carbon dynamics in the northern permafrost region on the trajectory of climate change, Proceedings of the National Academy of Sciences, 115, 3882, 10.1073/pnas.1719903115, 2018.

Meinshausen, M., Smith, S. J., Calvin, K., Daniel, J. S., Kainuma, M. L. T., Lamarque, J. F., Matsumoto, K., Montzka, S. A., Raper, S. C. B., Riahi, K., Thomson, A., Velders, G. J. M., and van Vuuren, D. P. P.: The RCP greenhouse gas concentrations and their extensions from 1765 to 2300, Climatic Change, 109, 213, 10.1007/s10584-011-0156-z, 2011.

Melton, J. R., Chan, E., Millard, K., Fortier, M., Winton, R. S., Martín-López, J. M., Cadillo-Quiroz, H., Kidd, D., and Verchot, L. V.: A map of global peatland extent created using machine learning (Peat-ML), Geosci. Model Dev. Discuss., 2022, 1-44, 10.5194/gmd-2021-426, 2022.

Miao, C., Duan, Q., Sun, Q., Huang, Y., Kong, D., Yang, T., Ye, A., Di, Z., and Gong, W.: Assessment of CMIP5 climate models and projected temperature changes over Northern Eurasia, Environmental Research Letters, 9, 055007, 10.1088/1748-9326/9/5/055007, 2014.

Müller, J. and Joos, F.: Committed and projected future changes in global peatlands – continued transient model simulations since the Last Glacial Maximum, Biogeosciences, 18, 3657-3687, 10.5194/bg-18-3657-2021, 2021.

Nichols, J. E. and Peteet, D. M.: Rapid expansion of northern peatlands and doubled estimate of carbon storage, Nature Geoscience, 12, 917-921, 10.1038/s41561-019-0454-z, 2019.

Niu, Z., Zhang, H., Wang, X., Yao, W., Zhou, D., Zhao, K., Zhao, H., Li, N., Huang, H., Li, C., Yang, J., Liu, C., Liu, S., Wang, L., Li, Z., Yang, Z., Qiao, F., Zheng, Y., Chen, Y., Sheng, Y., Gao, X., Zhu, W., Wang, W., Wang, H., Weng, Y., Zhuang, D., Liu, J., Luo, Z., Cheng, X., Guo, Z., and Gong, P.: Mapping wetland changes in China between 1978 and 2008, Chinese Science Bulletin, 57, 2813-2823, 10.1007/s11434-012-5093-3, 2012.

https://doi.org/10.5194/egusphere-2022-1006
Preprint. Discussion started: 30 September 2022


Obu, J., Westermann, S., Barboux, C., Bartsch, A., Delaloye, R., Grosse, G., Heim, B., Hugelius, G., Irrgang, A., Kääb, A. M., Kroisleitner, C., Matthes, H., Nitze, I., Pellet, C., Seifert, F. M., Strozzi, T., Wegmüller, U., Wieczorek, M., and Wiesmann, A.: ESA Permafrost Climate Change Initiative (Permafrost_cci): Permafrost Climate Research Data Package v1., Centre for Environmental Data Analysis [dataset], https://catalogue.ceda.ac.uk/uuid/1f88068e86304b0fbd34456115b6606f, 2020.

Palmer, M. D., Harris, G. R., and Gregory, J. M.: Extending CMIP5 projections of global mean temperature change and sea level rise due to thermal expansion using a physically-based emulator, Environmental Research Letters, 13, 084003, 10.1088/1748-9326/aad2e4, 2018.

Piao, S., Ciais, P., Friedlingstein, P., Peylin, P., Reichstein, M., Luyssaert, S., Margolis, H., Fang, J., Barr, A., Chen, A., Grelle, A., Hollinger, D. Y., Laurila, T., Lindroth, A., Richardson, A. D., and Vesala, T.: Net carbon dioxide losses of northern ecosystems in response to autumn warming, Nature, 451, 49-52, 10.1038/nature06444, 2008.

Qiu, C., Zhu, D., Ciais, P., Guenet, B., and Peng, S.: The role of northern peatlands in the global carbon cycle for the 21st century, Global Ecology and Biogeography, 29, 956-973, https://doi.org/10.1111/geb.13081, 2020.

Qiu, C., Zhu, D., Ciais, P., Guenet, B., Peng, S., Krinner, G., Tootchi, A., Ducharne, A., and Hastie, A.: Modelling northern peatland area and carbon dynamics since the Holocene with the ORCHIDEE-PEAT land surface model (SVN r5488), Geosci. Model Dev., 12, 2961-2982, 10.5194/gmd-12-2961-2019, 2019.

Qiu, C., Ciais, P., Zhu, D., Guenet, B., Chang, J., Chaudhary, N., Kleinen, T., Li, X., Müller, J., Xi, Y., Zhang, W., Ballantyne, A., Brewer, S. C., Brovkin, V., Charman, D. J., Gustafson, A., Gallego-Sala, A. V., Gasser, T., Holden, J., Joos, F., Kwon, M. J., Lauerwald, R., Miller, P. A., Peng, S., Page, S., Smith, B., Stocker, B. D., Sannel, A. B. K., Salmon, E., Schurgers, G., Shurpali, N. J., Wårlind, D., and Westermann, S.: A strong mitigation scenario maintains climate neutrality of northern peatlands, One Earth, https://doi.org/10.1016/j.oneear.2021.12.008, 2022.

Rawls, W. J., Ahuja, L. R., Brakensiek, D. L., and Shirmohammadi, A.: Infiltration and soil water movement, in, McGraw-Hill Inc., New York, 5.1-5.51, 1992.

Schaperow, J. and Li, D.: VICGlobal: soil and vegetation parameters for the Variable Infiltration Capacity hydrological model (1.6d) [dataset], https://doi.org/10.5281/zenodo.5038653, 2021.

Schneider von Deimling, T., Grosse, G., Strauss, J., Schirrmeister, L., Morgenstern, A., Schaphoff, S., Meinshausen, M., and Boike, J.: Observation-based modelling of permafrost carbon fluxes with accounting for deep carbon deposits and thermokarst activity, Biogeosciences, 12, 3469-3488, 10.5194/bg-12-3469-2015, 2015.

Schuur, E. A. G., McGuire, A. D., Schädel, C., Grosse, G., Harden, J. W., Hayes, D. J., Hugelius, G., Koven, C. D., Kuhry, P., Lawrence, D. M., Natali, S. M., Olefeldt, D., Romanovsky, V. E., Schaefer, K., Turetsky, M. R., Treat, C. C., and Vonk, J. E.: Climate change and the permafrost carbon feedback, Nature, 520, 171-179, 10.1038/nature14338, 2015.

Sheffield, J., Barrett, A., Colle, B., Fernando, D., Fu, R., Geil, K., Hu, Q., Kinter, J., Kumar, S., Langenbrunner, B., Lombardo, K., Long, L., Maloney, E., Mariotti, A., Meyerson, J., Mo, K., Neelin, J., Nigam, S., Pan, Z., and Yin, L.: North American Climate in CMIP5 Experiments. Part I: Evaluation of Historical Simulations of Continental and Regional Climatology*, Journal of Climate, 26, 9209-9245, 10.1175/JCLI-D-12-00592.1, 2013.

Smith, S. L., O'Neill, H. B., Isaksen, K., Noetzli, J., and Romanovsky, V. E.: The changing thermal state of permafrost, Nature Reviews Earth & Environment, 3, 10-23, 10.1038/s43017-021-00240-1, 2022.

Spahni, R., Joos, F., Stocker, B. D., Steinacher, M., and Yu, Z. C.: Transient simulations of the carbon and nitrogen dynamics in northern peatlands: from the Last Glacial Maximum to the 21st century, Clim. Past, 9, 1287-1308, 10.5194/cp-9-1287-2013, 2013.

Stocker, B. D., Spahni, R., and Joos, F.: DYPTOP: a cost-efficient TOPMODEL implementation to simulate sub-grid spatio-temporal dynamics of global wetlands and peatlands, Geosci. Model Dev., 7, 3089-3110, 10.5194/gmd-7-3089-2014, 2014.

Tang, R., He, B., Chen, H. W., Chen, D., Chen, Y., Fu, Y. H., Yuan, W., Li, B., Li, Z., Guo, L., Hao, X., Sun, L., Liu, H., Sun, C., and Yang, Y.: Increasing terrestrial ecosystem carbon release in response to autumn cooling and warming, Nature Climate Change, 12, 380-385, 10.1038/s41558-022-01304-w, 2022.

Tape, K. E. N., Sturm, M., and Racine, C.: The evidence for shrub expansion in Northern Alaska and the Pan-Arctic, Global Change Biology, 12, 686-702, https://doi.org/10.1111/j.1365-2486.2006.01128.x, 2006.

Treat, C. C., Jones, M. C., Brosius, L., Grosse, G., Walter Anthony, K., and Frolking, S.: The role of wetland expansion and successional processes in methane emissions from northern wetlands during the Holocene, Quaternary Science Reviews, 257, 106864, https://doi.org/10.1016/j.quascirev.2021.106864, 2021.
Turunen, J., Tomppo, E., Tolonen, K., and Reinikainen, A.: Estimating carbon accumulation rates of undrained mires in Finland–application to boreal and subarctic regions, The Holocene, 12, 69-80, 10.1191/0959683602hl522rp, 2002.
Wood, E. F., Lettenmaier, D. P., and Zartarian, V. G.: A land-surface hydrology parameterization with subgrid variability for general circulation models, Journal of Geophysical Research: Atmospheres, 97, 2717-2728, https://doi.org/10.1029/91JD01786, 1992.
Xu, J., Morris, P. J., Liu, J., and Holden, J.: PEATMAP: Refining estimates of global peatland distribution based on a meta-analysis, CATENA, 160, 134-140, https://doi.org/10.1016/j.catena.2017.09.010, 2018.
Yi, Y. and Kimball, J. S.: ABoVE: Active Layer Thickness from Remote Sensing Permafrost Model, Alaska, 2001-2015, 10.3334/ORNLDAAC/1760, 2020.
Yokohata, T., Saito, K., Ito, A., Ohno, H., Tanaka, K., Hajima, T., and Iwahana, G.: Future projection of greenhouse gas emissions due to permafrost degradation using a simple numerical scheme with a global land surface model, Progress in Earth and Planetary Science, 7, 56, 10.1186/s40645-020-00366-8, 2020.
Yu, Z., Beilman, D., and Jones, M.: Sensitivity of Northern Peatland Carbon Dynamics to Holocene Climate Change, Washington DC American Geophysical Union Geophysical Monograph Series, 184, 55-69, 10.1029/2008GM000822, 2009.
Zhao, B., Zhuang, Q., and Frolking, S.: Modeling carbon accumulation and greenhouse gas emissions of northern peatlands since the Holocene (in review), 2022a.
Zhao, B., Zhuang, Q., Treat, C., and Frolking, S.: A Model Intercomparison Analysis for Controls on C Accumulation in North American Peatlands, Journal of Geophysical Research: Biogeosciences, 127, e2021JG006762, https://doi.org/10.1029/2021JG006762, 2022b.
Zhao, R. J., Liu, X. R., and Singh, V. P.: The Xinanjiang model,
Zhuang, Q., McGuire, A. D., O'Neill, K. P., Harden, J. W., Romanovsky, V. E., and Yarie, J.: Modeling soil thermal and carbon dynamics of a fire chronosequence in interior Alaska, Journal of Geophysical Research: Atmospheres, 107, FFR 3-1-FFR 3-26, https://doi.org/10.1029/2001JD001244, 2002.
Zhuang, Q., Melillo, J. M., Kicklighter, D. W., Prinn, R. G., McGuire, A. D., Steudler, P. A., Felzer, B. S., and Hu, S.: Methane fluxes between terrestrial ecosystems and the atmosphere at northern high latitudes during the past century: A retrospective analysis with a process-based biogeochemistry model, Global Biogeochemical Cycles, 18, https://doi.org/10.1029/2004GB002239, 2004.
Zomer, R. J. and Trabucco, A.: Version 3 of the "Global Aridity Index and Potential Evapotranspiration (ET0) Database": Estimation of Penman-Monteith Reference Evapotranspiration. (In Press). [dataset], https://cgiarcsi.community/2019/01/24/globalaridity-index-and-potential-evapotranspiration-climate-database-v3/, 2022.

## Supplemental References

Hugelius, G., Loisel, J., Chadburn, S., Jackson, R. B., Jones, M., MacDonald, G., Marushchak, M., Olefeldt, D., Packalen, M., Siewert, M. B., Treat, C., Turetsky, M., Voigt, C., and Yu, Z.: Large stocks of peatland carbon and nitrogen are vulnerable to permafrost thaw, Proceedings of the National Academy of Sciences, 117, 20438, 10.1073/pnas.1916387117, 2020.
Melton, J. R., Chan, E., Millard, K., Fortier, M., Winton, R. S., Martín-López, J. M., Cadillo-Quiroz, H., Kidd, D., and Verchot, L. V.: A map of global peatland extent created using machine learning (Peat-ML), Geosci. Model Dev. Discuss., 2022, 1-44, 10.5194/gmd-2021-426, 2022.
Obu, J., Westermann, S., Barboux, C., Bartsch, A., Delaloye, R., Grosse, G., Heim, B., Hugelius, G., Irrgang, A., Kääb, A. M., Kroisleitner, C., Matthes, H., Nitze, I., Pellet, C., Seifert, F. M., Strozzi, T., Wegmüller, U., Wieczorek, M., and Wiesmann, A.: ESA Permafrost Climate Change Initiative (Permafrost_cci): Permafrost Climate Research Data Package v1., Centre for Environmental Data Analysis [dataset], https://catalogue.ceda.ac.uk/uuid/1f88068e86304b0fbd34456115b6606f, 2020.

https://doi.org/10.5194/egusphere-2022-1006
Preprint. Discussion started: 30 September 2022


Xu, J., Morris, P. J., Liu, J., and Holden, J.: PEATMAP: Refining estimates of global peatland distribution based on a meta-analysis, CATENA, 160, 134-140, https://doi.org/10.1016/j.catena.2017.09.010, 2018.

Yi, Y. and Kimball, J. S.: ABoVE: Active Layer Thickness from Remote Sensing Permafrost Model, Alaska, 2001-2015, 10.3334/ORNLDAAC/1760, 2020.

Zhao, B., Zhuang, Q., and Frolking, S.: Modeling carbon accumulation and greenhouse gas emissions of northern peatlands since the Holocene (in review), 2022.

Zomer, R. J. and Trabucco, A.: Version 3 of the "Global Aridity Index and Potential Evapotranspiration (ET0) Database": Estimation of Penman-Monteith Reference Evapotranspiration. (In Press). [dataset], https://cgiarcsi.community/2019/01/24/globalaridity-index-and-potential-evapotranspiration-climate-database-v3/, 2022.